JVST A
Journal of Vacuum Science & Technology A

Deep UV AlGaN LED reliability for long duration space missions

Cite as: J. Vac. Sci. Technol. A **41**, 013202 (2023); https://doi.org/10.1116/6.0002199
Submitted: 05 September 2022 • Accepted: 03 November 2022 • Published Online: 08 December 2022

Benjamin C. Letson, Simon Barke, Peter Wass, et al.

JVST A
Journal of Vacuum Science & Technology A
ARTICLE
avs.scitation.org/journal/jva

Deep UV AlGaN LED reliability for long duration space missions

Cite as: J. Vac. Sci. Technol. A **41**, 013202 (2023); doi: 10.1116/6.0002199
Submitted: 5 September 2022 · Accepted: 3 November 2022 ·
Published Online: 8 December 2022

View Online Export Citation CrossMark

Benjamin C. Letson,[1,a)] Simon Barke,[2] Peter Wass,[1] Guido Mueller,[2] Fan Ren,[3] Stephen J. Pearton,[4] and John W. Conklin[1]

AFFILIATIONS

[1]Department of Mechanical and Aerospace Engineering, University of Florida, Gainesville, Florida 32611
[2]Department of Physics, University of Florida, Gainesville, Florida 32611
[3]Department of Chemical Engineering, University of Florida, Gainesville, Florida 32611
[4]Department of Materials Science and Engineering, University of Florida, Gainesville, Florida 32611

[a)]**Electronic mail:** benletson27@gmail.com

ABSTRACT

Space-based gravitational wave detection will be carried out by the laser interferometer space antenna (LISA), a joint European Space Agency and NASA collaboration. The configuration of this antenna will include three identical spacecraft in a triangular formation separated by 2.5×10^6 km, flying in a drag-free formation around free-falling test masses. Charging of the test masses by cosmic ray fluxes and solar energetic particles must be compensated by photons that contain more energy than the effective work function of gold (4.3 ± 0.4 eV). The UV photons will be provided by AlGaN light emitting diodes, which must operate reliably for the duration of the mission. We have tested a large number (96 for dc and pulsed testing, more than 200 for all tests) of UV LEDs over a period of up to 600 days to characterize their performance over a wide range of operating conditions, assessing the lifetime performance under dc (1–80 mA drive current) and pulsed conditions (500–100 000 pulses per second) and temperatures ranging from 20 to 80 °C. Degradation of UV light output is faster at elevated temperatures and dc conditions. Preselection of LEDs based on initial spectral ratio of peak-to-midgap emission and ideality factor provides a positive correlation with subsequent reliability. The UV LEDs used for LISA will need to support 2 years of cruise and commissioning plus a 4-year baseline science mission.

I. INTRODUCTION

A. LISA

Laser interferometer space antenna (LISA) will be the first gravitational wave detector in space, allowing for the detection of gravitational waves with frequencies between 0.1 mHz and 1 Hz.[1–10] LISA will consist of three identical spacecraft flying in a drag-free formation around free-falling test masses (TMs).[1,6] The spacecraft will use laser interferometry to detect position changes of the test masses along the sensitive axis of each arm, requiring the TMs to be kept in a free-fall below the level of $1 \times 10^{-15} \frac{\mathrm{g}}{\sqrt{\mathrm{Hz}}}$ in the mHz band to allow for the detection of gravitational waves.[8,11–18] The TMs are surrounded by electrode housings, and the two make up the key components of the LISA inertial measurement sensor, called a gravitational reference sensor (GRS). Due to the charge buildup primarily caused by cosmic rays, LISA TMs will need to be discharged to minimize the effect of electrostatic forces on gravitational-wave observations. Utilizing the photoelectric effect, the gold-coated test masses can be discharged by illuminating their surfaces with photons of energy greater than the effective work function of gold. A pure gold surface has a work function of 5.1 eV, which would require light with a wavelength of ≈243 nm to eject electrons from the metal. However, surface contamination such as exposure to oxygen and hydrocarbons generally lowers the work function of gold to an average of 4.3 ± 0.4 eV, requiring less energetic photons to remove electrons from the surface.[10]

Contactless discharge using photoemission under illumination by ultraviolet light has been demonstrated several times in the past. Both Gravity Probe B[12,19] and LISA pathfinder (LPF)[13,14] demonstrated this using mercury-vapor lamps, but LISA will use state-of-the-art deep UV (DUV) LEDs[20–37] to achieve contactless charge control in both dc and pulsed illumination schemes.[7,8,38,39]

Since UV LEDs have never been used on a large class space mission before, they need to be space-qualified before LISA launches. Testing of over 200 UV LEDs has been performed to characterize both the short-term and long-term performance of the devices over the entire expected operating range of the LISA charge management device (CMD). The CMD consists of 12 UV LEDs, which will provide the UV light for contactless discharge of both TMs on the LISA spacecraft as well as the analog and digital electronics responsible for taking commands from the spacecraft and providing power to the UV LEDs.

Mercury vapor lamps have been used in several space missions previously because they were the only deep UV light source suitable for space operation until recently. Hg lamps have several characteristics that make their use undesirable. The lamps tend to have slow turn-on responses, high temperature sensitivity, and limited lifetimes. They also are significant sources of radio frequency interference and electromagnetic interference, and since their bulbs are made of glass, they require heavy structural reinforcement to survive the launch environment.[17]

Light emitting diodes (LEDs) are now available in the deep UV range ($\lambda < 280$ nm). UV LEDs are a potential successor to the Hg vapor lamps. They present advantages over Hg lamps because of their smaller size, lower weight, and lower electrical power consumption.[20–37] The high bandwidths of UV LEDs also allow them to be pulsed at frequencies up to 1 MHz, giving them a dynamic power range several orders of magnitude above what is capable with Hg lamps. In 2014, the Saudi-Sat 4 mission demonstrated space-borne utility of UV LEDs and UV LED charge management. Although the UV LEDs onboard Saudi-Sat 4 were only operated in low earth orbit for a period of about a month, the satellite did examine the effects of the space environment on LEDs over a 12-month period and demonstrated the ability of UV LEDs to change the charge of a gold proof mass.[18] A single LISA charge management device will feature 12 UV LEDs, which will replace the 6 Hg lamps previously used onboard the LISA Pathfinder.

B. Deep UV LED reliability

UV LEDs use aluminum gallium nitride, $Al_xGa_{1-x}N$, active layers.[40–53] Devices with the Al content up to $x = 0.45$ can produce light in the UV-B range (280–320 nm), while deep UV-C LEDs (peak wavelength emission below 280 nm) require Al contents approaching 70%. UV-C LEDs are of particular interest for the LISA charge management system since the wavelengths in this range achieve TM discharge via photoemission. DUV LEDs have been traditionally grown on sapphire substrates since sapphire is mostly transparent to DUV light. However, this choice of substrates typically leads to a large mismatch in the crystal lattice of the bulk and substrate materials. This causes higher threading dislocation densities (TDDs) in DUV LEDs[21] as well as a higher density of point defects such as hydrogen and carbon impurities or group-III vacancies (V_{Ga}, V_{Al}). These defects will act as recombination centers during electron-hole recombination, reducing LED efficiency.[32]

As an alternative, an AlN buffer layer can be used to grow AlGaN devices,[23,24] which serves as a transition layer to achieve better lattice match with sapphire and AlGaN and leads to a decrease in the TDDs of several orders of magnitude.[25] Crystal IS, one of two main commercial manufacturers of DUV LEDs, also employs pure AlN substrates to improve the crystal quality. Point defects are reported to cause most of the device degradation over time and optimized growth/fabrication methods that reduce the concentration of these defects are needed to increase the internal quantum efficiency, lifetime, and quality of DUV LEDs.[25]

Although blue and violet GaN-based LEDs show up to 50 000 h of stable operation,[27] UV LEDs have lower lifetimes. There are some recent reports on the physical processes that affect the degradation of UV-C LEDs and UV-B devices with similar structures but lower aluminum contents.[48,53] The defects that lead to decreased performance are related to the high concentrations of Al in AlGaN alloys. Degradation of AlGaN-based UV LEDs is at least partially due to the generation or the diffusion of point defects near the active region. These point defects can cause the generation of trap states. According to the Shockley–Read–Hall (SRH) theory, these trap states provide a path for electron-hole recombination that results in either nonradiative recombination or radiative recombination that produces a photon with a longer wavelength than the main spectral peak. Although both are possible, nonradiative recombination is a much more common effect of SRH recombination sites. Defects causing the trap states seem to diffuse from other areas of the semiconductor to near the active area, where they negatively impact the device efficiency. This is a diffusion process because changes in the ideality factor, intensity in different spectrum peaks, and reverse leakage current all follow a $t^{1/2}$ dependency after more than 50 h of constant current stress.[48,53] The LED's deterioration is related to the generation or migration of these point defects, with the optical power output more affected at lower current driving conditions than higher driving conditions.[30–32] Trap-assisted recombination will affect power output at lower drive currents more than at higher drive currents since the concentration of defects is a large fraction of the total recombination sites active at low drive currents. As the drive current increases, the total number of recombination centers saturates and represents a smaller fraction of the total electron-hole recombination occurring in the device. While there is still some uncertainty on the exact mechanisms causing the gradual power decline of UV LEDs, there is a consensus that the presence and migration of defects within the semiconductor lattice is a contributor.

II. DEGRADATION OF UV LEDs

The first indicator of UV LED quality is the optical spectrum. If electrons have an alternative route to recombine with holes other than from within the quantum wells, a secondary parasitic peak forms. Defects can provide electron-hole recombination paths resulting in photon emission at a longer wavelength than the main peak. Several studies[26–37,40–48] monitoring spectral changes in multiple devices over long periods of constant current stress detected a parasitic peak attributed to defect-assisted radiative recombination near the active region. The quality of a device spectrum is a good indication of which recombination processes are taking place.

Another indication of the device quality is the ideality factor. The current-voltage (I–V) relationship of a general Schottky diode

is given by

$$I = I_0\left(\exp\left(\frac{qV}{nk_BT}\right) - 1\right), \tag{1}$$

where I is the diode current, I_0 is the diode reverse saturation current, q is the unit charge, V is the diode voltage, k_B is Boltzmann's constant, and T is the temperature of the device junction. The unitless diode ideality factor, n, is added to the ideal Schottky diode equation to account for nonideal device behavior. UV LEDs are commonly observed to have ideality factors of up to 7, indicating the presence of numerous conduction mechanisms.[50–52] Although AlGaN devices exhibit ideality factors higher than theory initially predicts, this metric can still be used to assess the LED quality compared to other DUV LEDs. A lower device ideality factor should still indicate that the diode current is being produced by direct electron-hole recombination. In contrast, higher ideality factors indicate more recombination occurring via recombination sites resulting from the presence of defects. The ideality factor can be determined experimentally from a voltage-current sweep by fitting a line to the linear region of $\ln(I)$ vs V, where the slope is equal to $\frac{q}{nk_bT}$. This linear region generally occurs directly after device turn-on at low currents, as shown in Fig. 1(a). This will be referred to as the ideality factor in the on-region (IF_{on}).

Another device metric used to assess LED quality is the device's turn-on current, defined as the lowest current at which the LED starts to produce light. An increased turn-on current indicates higher levels of trap-assisted tunneling (TAT). This occurs when electrons cross the potential barrier of the semiconductor by trap-assisted conduction, generally due to deep traps present in the QWs with an energy level near the midgap that assists the tunneling mechanism. Monti *et al.*[48,53] reported the current below turn-on increases with the square-root of stress time. This dependence indicates that the TAT mechanism is related to the diffusion of defects from inactive regions to active regions of the semiconductor. This can also be monitored by analyzing a second linear region in the I–V curve. An ideality factor in the off region (IF_{off}) can also be determined in a similar way to IF_{on}. This ideality factor can be used to track the turn-on current in the device, and as a result, an estimate of the number of defects contributing to TAT within the device.

While the current produced before turn-on is sometimes referred to as the forward leakage current, the reverse leakage current is a measure of the current produced in the negative direction when a diode is under reverse bias. The presence of point defects within or around the active region can cause a defect-assisted carrier transport where these traps allow for electrons to traverse the barrier region in the opposite direction and create a reverse current within the device. The leakage current has been shown to increase with stress time in the same studies that analyzed the increase in the turn-on current and is considered to be affected by the same defect diffusion or generation process that causes an increase in turn-on current.

The final metric used to assess the quality of the LEDs is the optical power output. Differences in power output between devices can be a result of a number of the effects previously discussed,

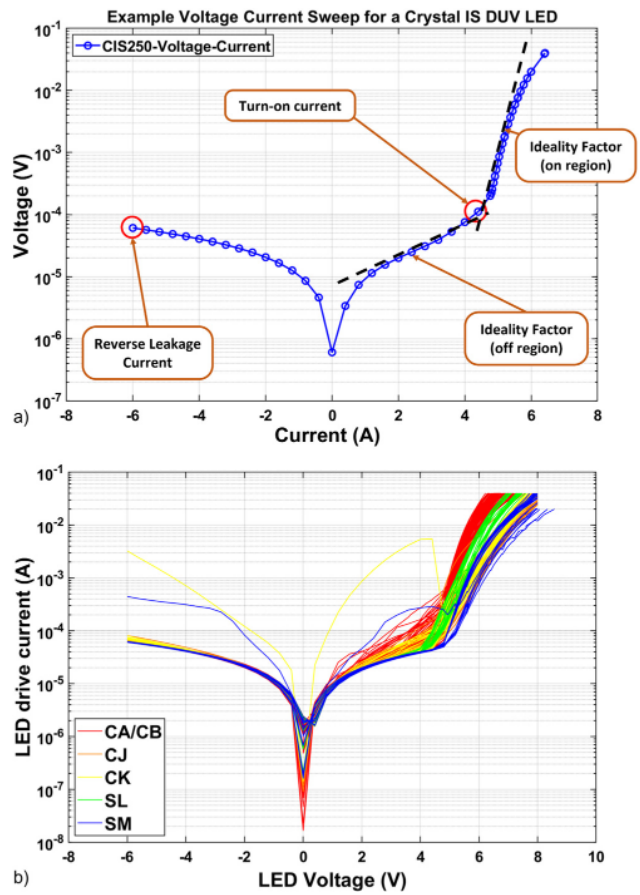

FIG. 1. (a) Indicators of the LED quality determined from a I–V sweep. (b) Pretest voltage-current sweeps for 120 CA and CB LEDs (see Table I).

specifically QW overflow, which reduces the number of electrons and holes that can recombine to produce photons, as well as the number of defects that contribute to nonradiative recombination within the device. One of the main effects contributing to power loss is the SRH recombination. By monitoring the optical power at a range of drive currents, the contribution of SRH recombination can be monitored.

III. EXPERIMENT

To understand the current state of commercial UV LEDs, large numbers need to be tested across a range of temperatures while operating in air and under vacuum. There are currently two commercial vendors for UVC LEDs: Crystal IS (CIS) supplying LEDs with wavelengths down to 250 nm,[54] and Sensor Electronic Technologies Inc. (SETi) supplying LEDs with peak wavelengths of 245 and 255 nm.[55] All these devices that were procured are packaged in a hermetic TO-39 can with a ball lens to provide heat sinking and to focus the light output. Although surface mount

TABLE I. Device details of all five batches used in the UV LED performance tests.

Internal ID	Manufacturer	Part No.	Lot No.	Quantity	Nominal peak wavelength (nm)
CJ	Crystal IS	OPTAN 250J-BL	A019C1	35	250
CK	Crystal IS	OPTAN 250J-BL	A017A1	27	250
SL	SETi	TUD59H1B	—	25	255
SM	SETi	TCE49H1B	—	25	245
CA	Crystal IS	OPTAN 250J-BL	UA2001-1-1 Box 1	60	250
CB	Crystal IS	OPTAN 250J-BL	UA2001-1-1 Box 2	60	250

packages are more commonly used with these UV LEDs, the ball lens packaging allows the light to be sufficiently focused into a fiber optic cable without needing to use additional optics inside the CMD. Five batches of UV LEDs were purchased, and various subsets of these batches have been put through performance testing, initial lifetime testing, and constant power lifetime testing. Details for each of the five batches are listed in Table I, as well as the internal serial number prefix that was given to each batch. The compilation of all the device I–V curves is shown in Fig. 1(b), showing differences in the forward I–V might be predictive of the presence of defects prior to device aging under bias. Figure 2 shows histograms of the leakage current at −6 V bias as well as the ideality factors discussed above. The unphysically large ideality factors shown indicate the presence of multiple current conduction mechanisms in these devices.

In the first set of UV LED performance tests, 112 UV LEDs were initially acquired from four lots of devices manufactured by the two vendors. These four lots will be referred to as CJ, CK, SL, and SM and details about each lot are given in Table I. After initial spectrum and current sweep measurements were made on all LEDs at 20 °C, the eight devices with the lowest secondary emission peak and the eight devices with the highest secondary emission peak were chosen from each lot to be put through a more comprehensive set of performance tests. Detailed results of these performance tests are reported in Ref. 56. To test the reliability of these four types of devices and get an idea of which parameters affected the degradation rates the most, 96 LEDs (24 from each type) were tested at four temperatures, 20, 40, 60, and 80 °C. The wide temperature range was selected in an effort to extract a temperature-dependant activation energy for each type of device at each operating mode, similar to the work done at Imperial College London by Hollington *et al.*[57] This work will be briefly discussed in Sec. IV C. At each temperature, devices were tested at either a low, medium, or high stress driving condition in either a DC or pulsed manner. The devices being run in a DC, or continuous, mode were operated at either 1, 20, or 80 mA. The pulsed devices were operated at a driving current of 20 mA and a duty cycle of 5%, or a pulse width of 500 ns. The stress level was varied for each testing group by limiting the number of cycles of the 100 kHz reference signal in which a UV light pulse was produced. The low stress and medium stress devices only produced a UV pulse in the first 500 cycles and 10 000 cycles of every second, respectively. In contrast, the high-stress case devices pulsed continuously, meaning they produced a pulse in every cycle of the 100 kHz reference signal.

A second reliability test of the UV LEDs was performed on a new lot of CIS 250 nm LEDs (lots CA and CB). This second lifetime test was designed to perform an in-depth investigation of the low light output performance of 96 devices from the same lot. The statistics obtained from this test should give an accurate assessment of not only the inter-lot variability of the CIS 250 nm devices but also a direct assessment of whether these devices could perform continuous discharge for the duration of the LISA mission. After initial screening tests were performed looking at device metrics that could be calculated from a current sweep, voltage sweep, and DC spectra of each device, 96 devices were broken up into four groups that displayed roughly equal distributions of each of the parameters that were measured pretest. In this test, the devices were either tested in a low power, quasi-DC (1 Hz pulse width modulation) mode or a low power pulsed mode at either 20 or 40 °C. The quasi-DC (qDC) devices were driven in such a way that the LEDs would output a 1 s average power of 1 nW, and the pulsed devices were driven in such a way that the LEDs would output a 1 s average power of 4 nW. Both of these numbers are two times higher than the corresponding UV power requirements for these modes specified for the LISA CMD.

In both experiments, the continuous power monitoring of the 96 devices is done by SiC based, TOCON UV photodiodes with built in amplifiers. The UV LED test stand is operated by a dedicated National Instruments machine responsible for the commanding of the driving electronics and temperature controllers and monitoring of the average current, average voltage, and average optical power from each of the 96 UV LEDs. The test stand setup is detailed further in Ref. 56. Before the start of each lifetime test, pretest measurements were performed to characterize the current-voltage-power (IVP) curve as well as the optical spectrum of each UV LED. Figure 3 shows a comparison of the I–V curve (a) and the optical spectrum of each device at 20 mA (b).

IV. RESULTS AND DISCUSSION

The UV LEDs should be able to support test mass discharging in several different illumination methods, which are summarized in Table II. The intermittent discharge modes require the UV LEDs to produce relatively high powers of light for a short period of time. During these modes, the electric potential of the LISA TM would be brought from some upper potential to some lower potential, nominally +600 to −600 eV in a short amount of time. These discharge modes would keep the TM charge close enough to neutral that the electrostatic forces on the TM do not affect the LISA science measurement, but would not require the TM to be continuously illuminated. On the other hand, the continuous discharge

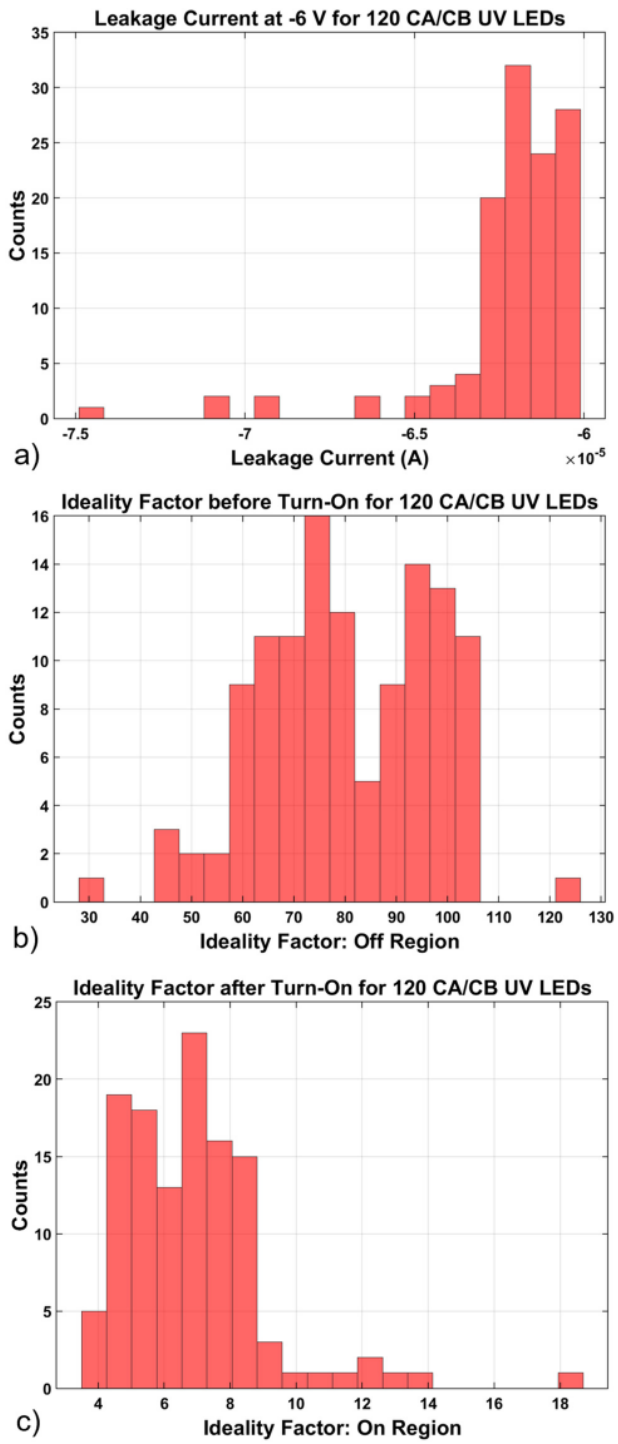

FIG. 2. Histograms of the (a) leakage current at −6 V, (b) IF*off*, and (c) IF*on* pretest properties calculated from voltage-current sweeps of 120 CIS LEDs from the CA and CB lots (see Table I).

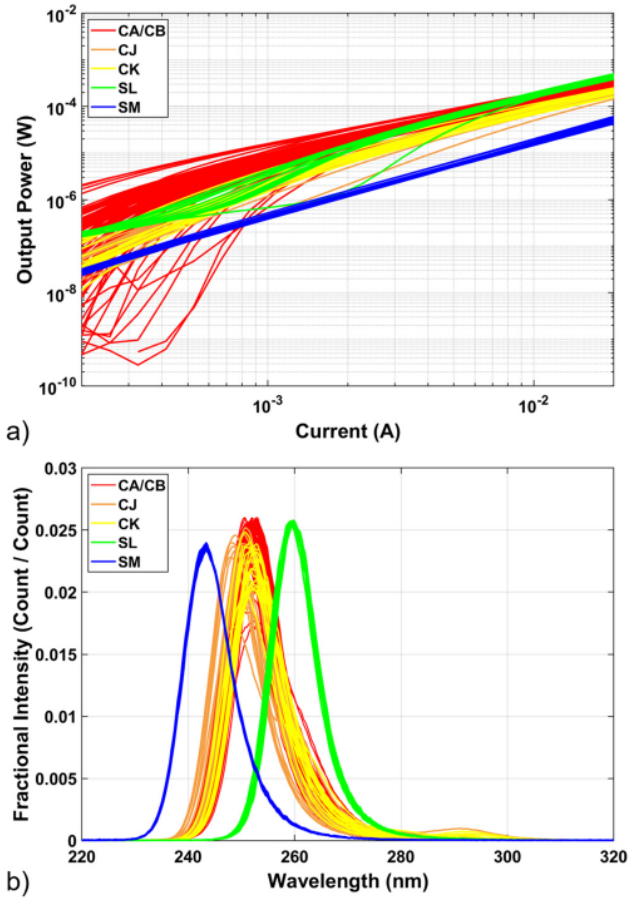

FIG. 3. (a) Pretest current-power curves for all five types of LEDs used in the lifetime tests. (b) Optical spectra of all five types of LEDs driven continuously at 20 mA.

TABLE II. Breakdown of the six operational discharge modes that can be used on LISA.

	Discharge modes	Continuous/ intermittent	Pulsed/ DC	UV power (nW)	Frac. on time
1	Timed	Intermittent	Pulsed	39	0.002
2	Low-power	Continuous	Pulsed	0.02	1
3	Phase control	Continuous	Pulsed	2	1
4	Timed	Intermittent	DC	26	0.003
5	High power equilibrium	Intermittent	DC	500	0.0002
6	Low power equilibrium	Continuous	DC/qDC	0.5	1

modes would require the UV LEDs to produce a very low average output power that would be tuned to exactly offset the environmental charging rate of the TM. Both continuous and intermittent discharge can be performed using pulsed and DC light, so there are a total of six discharge modes that the UV LEDs are required to support. The initial parameter survey lifetime test set out to look at the high and low power DC and pulsed discharge modes and also added a third test set to the pulsed and DC cases to be able to get a better idea of the effect that the driving stress had on the degradation rate of the LEDs.

A. Aging under DC conditions

The parameter survey lifetime test took place over 191 days while 96 UV LEDs were driven in 24 different operating modes and the output power was continuously monitored for each LED. Because the starting power for each device was slightly different, the data were normalized by the power at the beginning of the lifetime test to show relative power loss. Specifically, each curve was normalized by the average ADC output between 40 000 and 60 000 s from the start of the test. This allows for any temperature-dependent power fluctuations to settle as the rack and LEDs came up to their specified operating temperature.

Figure 4 shows the results from the DC 1 mA operating conditions for all four LED types and all four operating temperatures. This low power operating condition is designed to represent a DC low power mode (mode 6) where a single UV LED will run continuously to perfectly match the test mass's environmental charging rate and maintain a low TM charge. In the continuous discharge modes, UV LEDs onboard LISA will be required to be operational 100% of the time, meaning the LEDs will need to be on for the entire 4 year science mission. Conservative estimates based on LISA Pathfinder data show that in a worst-case scenario, an intermittent discharge cycle of duration 600 s will be needed once every 3.5 days to keep the TM charge close enough to neutral. In this worst case scenario, the LED will only experience 9 days of on time over the course of a 12.5 year mission. Using these conservative estimates, the data from Fig. 5, which most closely represents discharge mode 5, show that all LEDs close to or below the recommended maximum operating temperature of the manufacturer (55 °C) survived for over 15 LISA lifetimes at 20 mA drive current, and many of these devices maintained 50% of their initial operating power well past 100 days of continuous operation. It is also worth noting that the errant behavior of the 20 °C SL device in Fig. 5(c) was determined to be due to an unreliable electrical connection on the current source of that device and was not due to a faulty LED.

Figure 6 shows the results of the DC 80 mA operating case. While 80 mA is well above the expected operating current of these devices, it is meant to gauge the bias dependent degradation of the UV LEDs at an extreme driving current. While the CJ and CK devices were relatively resilient to the extreme currents, the SL and SM devices showed a different behavior. In most of the test groups,

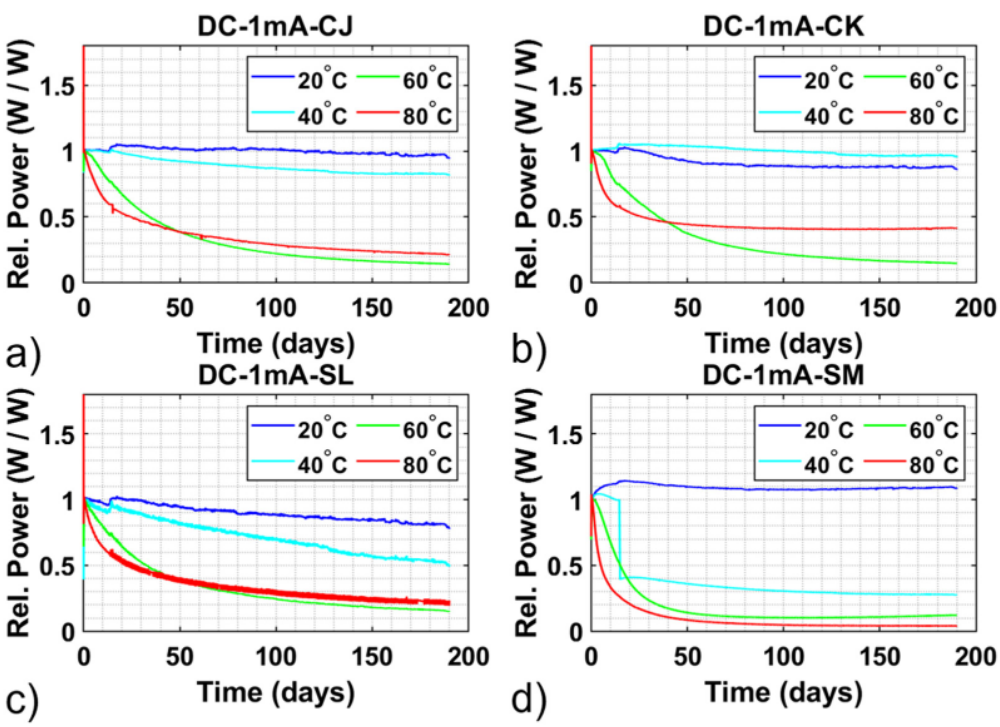

FIG. 4. Long-term aging at the DC 1 mA operating conditions for the CJ (a), CK (b), SL (c), and SM (d) LEDs at 20, 40, 60, and 80 °C.

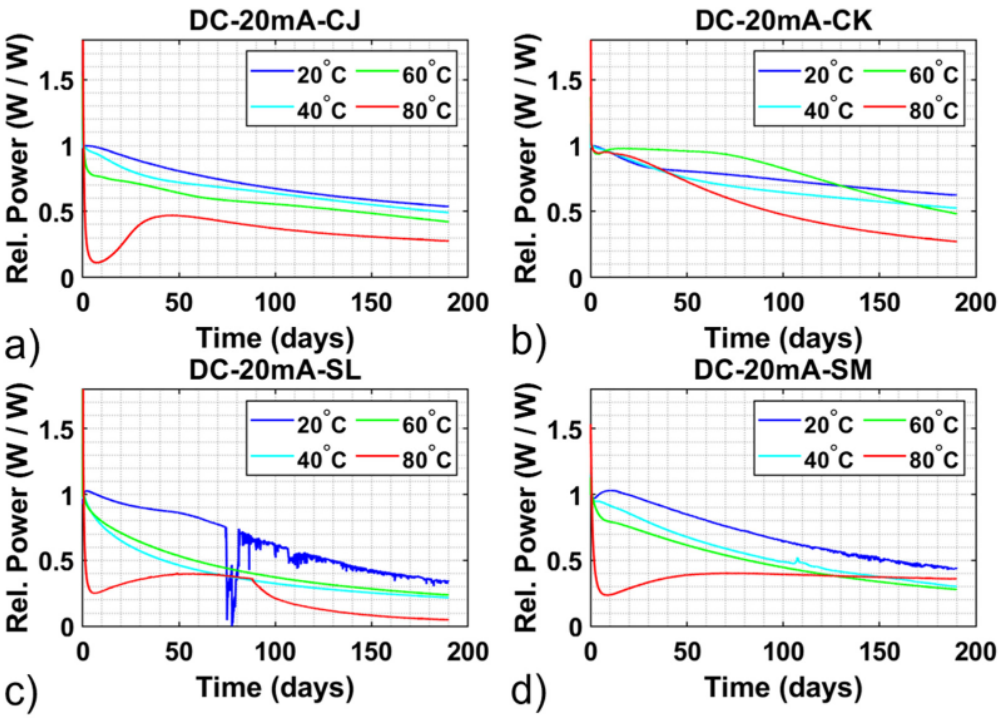

FIG. 5. Long-term aging at the DC 20 mA operating conditions for the CJ (a), CK (b), SL (c), and SM (d) LEDs at 20, 40, 60, and 80 °C.

the devices show a gradual decline from the beginning to the end of the test. In the high stress DC group, however, the SETi devices showed a rapid loss of power in the first 10 days and then reached an equilibrium and a much more gradual decline in output power. The manufacturer's recommended maximum operating current for these devices is only 20 mA compared to the Crystal IS maximum operating current of 100 mA. This could be attributed to the different behavior seen in this case compared to the other operating cases.

B. Aging under pulsed conditions

The pulsed 500 pulses per second (PPS) operating condition is meant to emulate the pulsed continuous discharge mode (mode 3) where the UV LED is operational for 100% of the mission. Although the devices shown in Fig. 7 were only operated for 177 days, none of the CIS devices at any temperature showed more than a 3% loss in power. Of the SETi devices tested, only the devices being run above the maximum recommended operating temperature declined by a noticeable amount. The dropout in the 20 °C devices from Fig. 7 is due to a momentary glitch in the power readback electronics and is not reflective of an actual loss of power in the devices. The excess noise seen in the 80 °C "SL" device, however, seems to be due to relatively large fluctuations in the average power of this one device that were present throughout the test and may indicate an unstable SETi 255 nm device.

Figure 8 shows the results of the pulsed, 10 000 PPS devices. While this case does not directly simulate any expected operating scenario for LISA, it does provide a medium stressed case for the pulsed devices. In some cases, the high-temperature devices lost a significant amount of their power during the 177-day test, however the low-temperature devices from all lots were relatively unaffected. The degradation of these LEDs being operated at 10 000 PPS also fell between the degradation of the 500 PPS LEDs and 100 000 PPS LEDs at a given temperature, indicating that the commanded pulses per second, or on time of the device, is a key factor that determines the degradation rate of these devices.

The pulsed 100 000 PPS operating case most closely simulates the pulsed intermittent discharge case or mode 1. Again, the UV LED would only need to be on for approximately 9 days during a 12.5-year LISA mission in this operating scenario. The data in Fig. 9 shows that all devices except the high-temperature SM devices would maintain more than 50% of their initial power for the required 9 days. Of those devices, the devices below 80 °C would survive for at least 15 LISA lifetimes while being operated in this discharge mode.

C. Lifetime degradation model development

The results of the parameter survey lifetime tests directly verify that UV LEDs will survive for the duration of the LISA mission if used in either of the intermittent discharge modes.

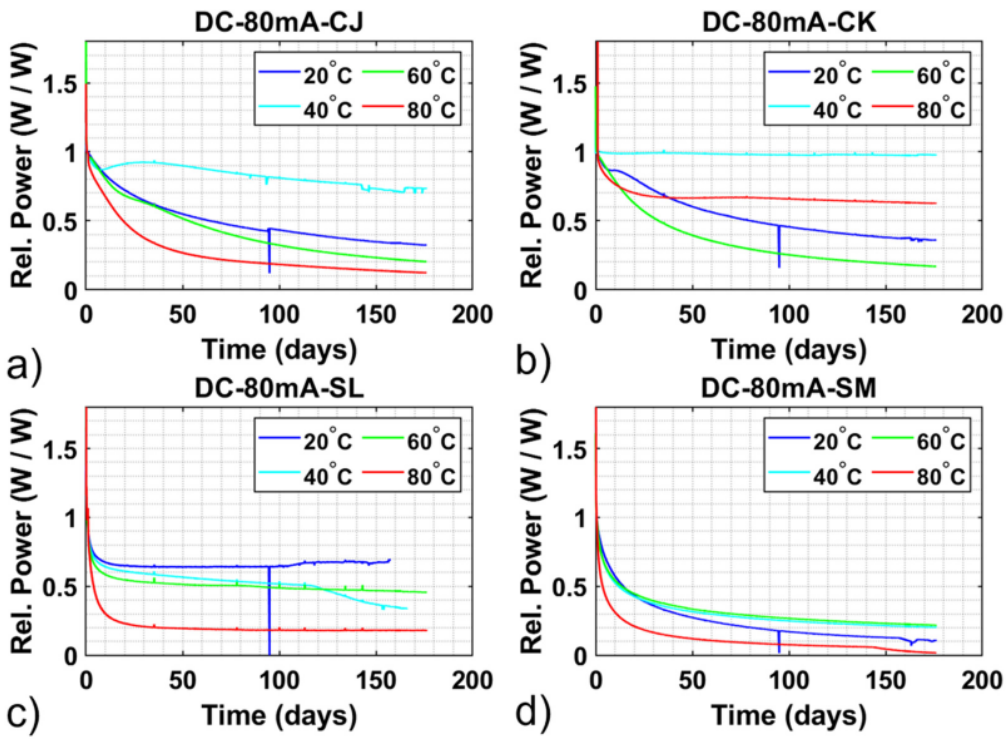

FIG. 6. Long-term aging at the DC 80 mA operating conditions for the CJ (a), CK (b), SL (c), and SM (d) LEDs at 20, 40, 60, and 80 °C.

However, the test was not long enough to directly show that the continuous modes will be possible for the first 6 years of the mission. We attempted to develop a model of the device degradation that is dependent on the stress time, driving conditions, and operating temperature of the device. Previous works[57,58] have used a double exponential model in the form of Eq. (2), where β_1 is a temperature dependent degradation constant and β_2 is a bias dependent degradation constant. P_0 is the device's initial power, but typically the P_0 term is dropped, and the equation is used to determine the normalized power loss in a device. The degradation constants β_1 and β_2 are typically separated by at least two orders of magnitude, with the temperature dependent β_1 typically driving the fast decay and the bias dependent β_2 typically determining the more gradual long term decay. The A_1 term is a unitless constant indicating whether the degradation is dominated by the faster time constant or the slower time constant,

$$P(t) = P_0(A_1 e^{-\beta_1 t} + (1 - A_1)e^{-\beta_2 t)}). \tag{2}$$

As β_1 is typically expressed as a temperature dependent degradation constant, an Arrhenius model is used to describe the relationship between junction temperature and decay rate of the output power.[58] In the Arrhenius model expressed in Eq. (3), k_b is Boltzmann's constant, T is the absolute junction temperature of the device, A_0 is a scaling constant, and E_a is the activation energy of that device,

$$\beta_1 = A_0 e^{\frac{E_a}{k_b T}}. \tag{3}$$

While this method has been used to extract a temperature dependent activation energy from LEDs in the past, the design of this initial lifetime test provided no statistics at a single operating mode for a single type of device, which left the results of the Arrhenius analysis sensitive to variations from device to device, which are amplified by the difficulty in manufacturing these high aluminum content devices that suffer from a high concentration of crystal lattice defects. Another issue with running an Arrhenius analysis on this test set is that two of the four test cases for a single device type were run at temperatures above the recommended maximum operating temperature of the UV LEDs. While longer wavelength LEDs do not require low operating temperatures below 55 °C, these DUV LEDs can exhibit failure mechanisms at high temperatures that would otherwise not be present at acceptable temperatures. By comparing devices at such a wide range of temperatures, the Arrhenius analysis was not successful at extracting a reliable activation energy from most of the test cases in this lifetime test. The shortcomings of this approach in terms of accurately obtaining the activation energy led us to try a more general Monte Carlo reliability analysis. Equation (2) still provides an accurate representation of the degradation rates of the LEDs, even if no clear

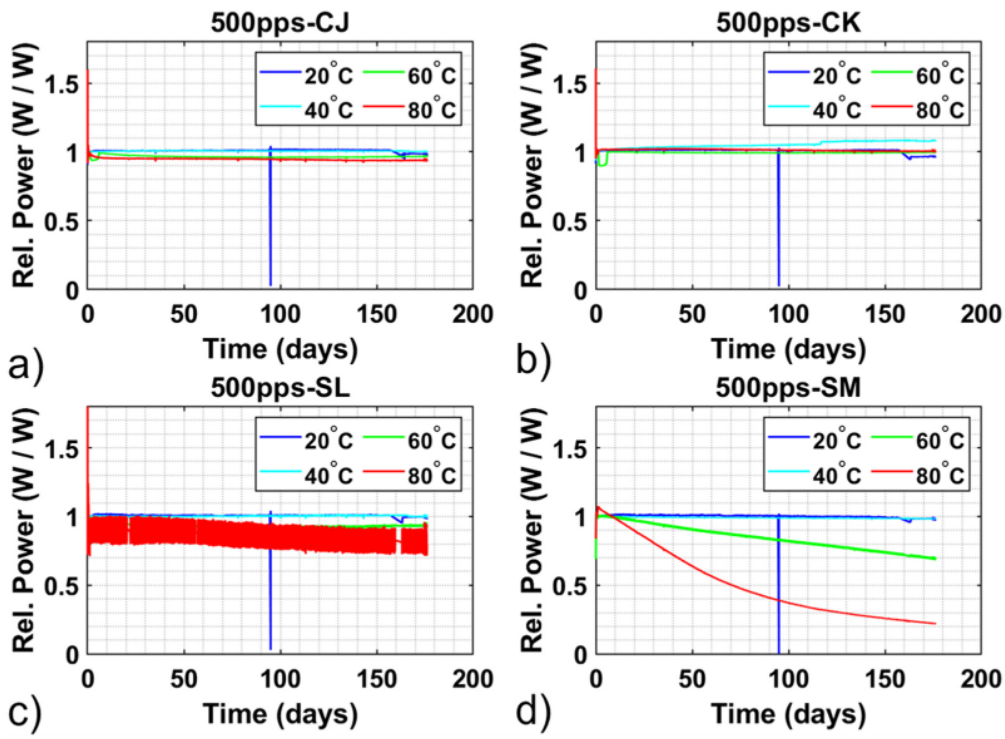

FIG. 7. Long-term aging at the Pulsed 500 PPS operating conditions for the CJ (a), CK (b), SL (c), and SM (d) LEDs at 20, 40, 60, and 80 °C.

relationship between the decay rate and operating temperature could be made for the different types of LEDs. Because of this, sample statistics of the A_1, β_1, and β_2 parameters were determined from the experimental data and used to generate a large number of sample LEDs for the Monte Carlo simulation. Results from all four device types at realistic spacecraft temperatures of 20 and 40 °C were combined to generate a larger sample size and provide an estimate of the degradation variability of a large number of devices. By expressing the average parameters as functions of either the forward voltage for the DC cases or the base 10 logarithm of the pulses per second for the pulsed cases, a general linear model was developed that related the average values of A_1, β_1, and β_2 to the operating condition of a set of devices.

After determining the means and covariances for the A_1, β_1, and β_2 parameters, 10 000 devices were generated and simulated in time until their power output had fallen below 30% of the initial power. Figure 10(a) shows the results of the Monte Carlo simulation of the DC continuous discharge mode. The vertical black lines mark the 5%, 10%, 25%, and 50% failure times of the devices, where failure is defined as when the output power falls below 30% of the device's initial output power, marked by the horizontal red line. The experimental data from the LEDs tested at 20 and 40 °C are also shown on top of the simulated output as a reference.

The simulation shows that 95% of the LEDs survive at least 527 days of DC continuous discharge, with 50% of the devices lasting over 1400 days. This simulation also shows that if eight devices were available per spacecraft, there would be 95% confidence that the eight devices would provide more than 12 years of DC continuous discharge for LISA. While the behavior of the simulated DC 1 mA LEDs do vary significantly, the results agree well with experimental data. The high variability likely comes from the fact that four different device types at two temperatures are used to generate the parameter distributions from which the 10 000 devices are sampled. This high variability is not likely to be seen in the single batch of LEDs from which the flight devices will be selected, so this method should provide a conservative estimate of the lifetimes of these devices.

Figure 10(b) shows the results of the Monte Carlo simulation for the pulsed continuous discharge mode. This shows that devices operated in the pulsed continuous discharge mode should last much longer than in the DC continuous mode, with 95% of simulated devices lasting over 8 years. The full table of failure percentiles for the DC and pulsed simulations are given in Table III. This simulation does indicate high confidence that the pulsed continuous discharge mode is feasible for the 4-year science mission target for LISA.

D. Constant power lifetime tests

While the parameter survey lifetime test was a good initial scan of the long term performance of a larger set of devices than

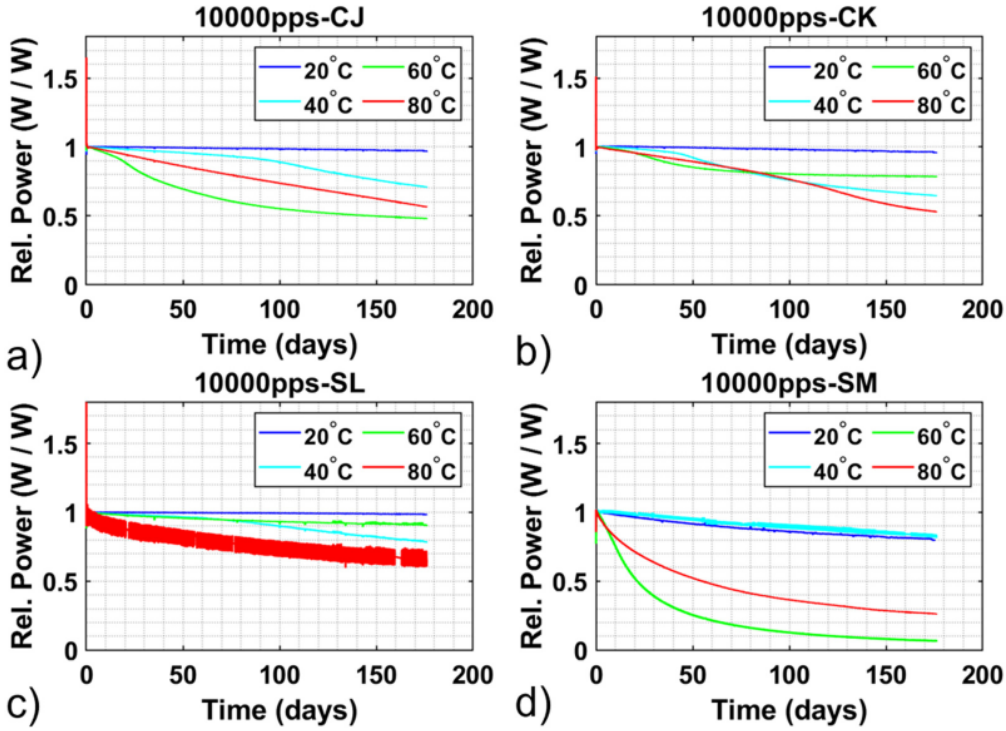

FIG. 8. Long-term aging at the pulsed 10 000 PPS operating conditions for the CJ (a), CK (b), SL (c), and SM (d) LEDs at 20, 40, 60, and 80 °C.

what has been tested before in the literature, the design of the test brought on several complications in data analysis that prevented a high confidence evaluation of the continuous operating modes. Thus, a new lifetime experiment was designed that featured redesigned testing software and a new set of 96 UV LEDs that will only be operated in either the pulsed continuous discharge mode (mode 3) or in a new, quasi-DC (qDC) operating mode as at realistic temperatures. The qDC operating mode can be thought of as a 1 Hz pulse width modulation (PWM) and replaces the dc continuous mode with the hope that the PWM of the LED output will allow for a more precise control of the output power without needing to operate the devices at low drive currents. The qDC mode should also show lifetime improvements over the low power DC mode since the total on-time of the device can be reduced, even though it does require operation at a higher drive current than the 1 mA case from the parameter survey lifetime test.

Since the only metric that matters in terms of UV LED lifetime for the LISA mission is the ability of the UV LED to produce enough power to effectively discharge the test mass, the driving parameters required to do so do not necessarily need to be locked in place. If an LED begins to lose output power over time, the driving parameters can simply be increased to ensure the device provides enough UV power to discharge the test mass. The redesigned LabVIEW test software features an output power feedback controller that will adjust the set voltage and pulses per second of each LED individually to regulate the output power of each device around the initial power levels at the start of the lifetime test. Since the measured output of the UV LEDs will no longer be following a double exponential decay while the controller is constantly changing the driving parameters, another metric needs to be used to track the progression of the UV LEDs over the course of the lifetime test. To do this, the constant power lifetime test uses a proposed metric that we call the integrated current (IC). The IC metric is the 1 s average current of each device and is computed as the product of the set current, duty cycle, and pulses per second divided by 100 000. This gives a value to how hard each LED needs to be driven per second to meet the target lifetime power level.

Continuous discharge power requirements for LISA dictate that power levels of 0.5 nW in the qDC mode and 2 nW in the pulsed mode should be maintained for the duration of the mission. To add margin to our test cases, the qDC and pulsed driving parameters were selected to maintain these target powers with a 2× margin (1 nW qDC and 4 nW pulsed). This lifetime experiment tested devices at only 2 temperatures; a nominal operating temperature of 20 °C and a more stressing temperature of 40 °C. This second temperature adds 10 °C of margin to the maximum operating temperature of the LISA CMD, but does not test the UV LEDs above their maximum operating temperature where failure mechanisms not present at expected spacecraft temperatures could be activated. 120 new Crystal IS 250 nm UV LEDs (internal IDs CA and CB

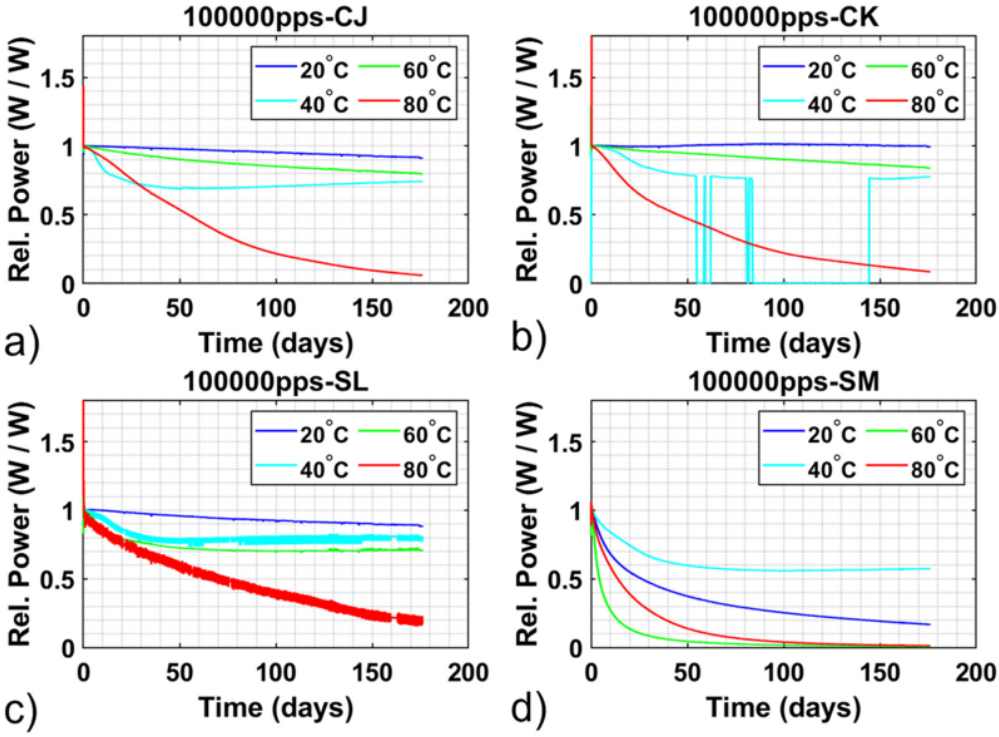

FIG. 9. Long-term aging at the pulsed 100 000 PPS operating conditions for the CJ (a), CK (b), SL (c), and SM (d) LEDs at 20, 40, 60, and 80 °C.

from Table I) were screened before, 96 devices were selected for use in the constant power lifetime tests.

The qDC continuous discharge parameters were selected so that the LEDs produced enough light to illuminate the TM with ≈1 nW. Once on the orbit inside of the LISA spacecraft, this will correspond to an initial driving current of 20 mA and 100 pulses per second or a qDC duty cycle of 0.1%. This means that the starting integrated current in the qDC mode was 0.02 mA s. For reference, an integrated current of 20 mA s would represent operation at DC 20 mA, so the qDC integrated current could be increased by at least a factor of 1000 if needed to achieve the necessary power levels.

The relative integrated current of the qDC 20 and 40 °C lifetime LEDs through 600 days of testing are shown in Fig. 11. At 20 °C, a small number of the LEDs actually showed a small increase in power. Device temperature was found to have a clear effect on the power loss of these devices. At the higher temperature, most devices required 2%–25% more integrated current, with 5 of the 24 tested devices requiring 35%–60% more integrated current to maintain their initial power levels. Even in the worst case, a relative IC of 1.6 for the qDC case equates to 20 mA driving current and a qDC duty cycle of 0.16%, which is well below the limits the LEDs can be driven.

For pulsed continuous discharge, the driving parameters of the pulsed LEDs were selected so this group of LEDs would produce 4 nW of optical power at the TM after estimated losses were accounted for. The LEDs began at a drive current of 20 mA, duty cycle of 10%, and 2000 pulses per second, which equates to a starting IC of 0.04 mA s. If the duty cycle is to remain at 10% for continuous discharge, the LEDs can still be driven by an integrated current of at least 2 mA s, which would correspond to being pulsed continuously at 20 mA and 10% duty cycle, or 50 times more integrated current than used at the start of the test. Both 20 and 40 °C test groups show less than 12% increases in integrated current after 600 days of testing, as shown in Fig. 12.

E. Parameter correlations

We also attempted to find correlations between the pretest metrics and lifetime performance. The pretest metrics used in the correlation analysis, as well as their correlation values sorted by operating case are shown in Table IV. These values are broken down by test group because the operating mode (qDC or pulsed) as well as operating temperature have an impact on the degradation of the LEDs, as evidenced by the parameter survey lifetime tests and the results of the constant power lifetime tests. By analyzing the correlations per test group, we isolated the impact of each metric.

As seen in the table, there were no parameters that consistently indicate a strong influence ($\rho > 0.7$) on the long-term performance of the LEDs in every operating mode. The more

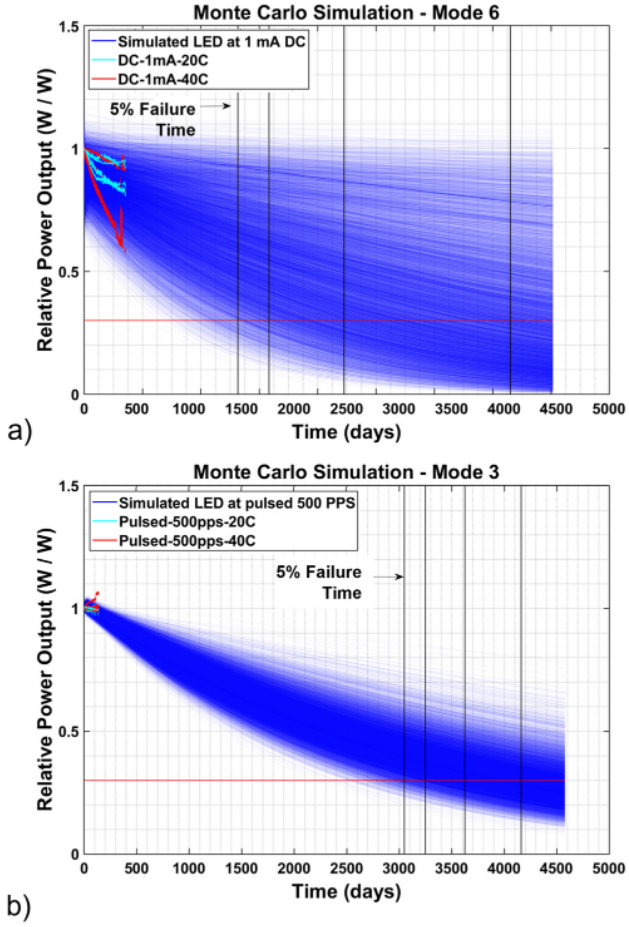

FIG. 10. Monte Carlo simulation of 10 000 UV LEDs operated in (a) the DC continuous discharge mode and (b) the pulsed continuous discharge mode. Experimental data from the 20 and 40 °C cases are plotted on top of the simulated devices.

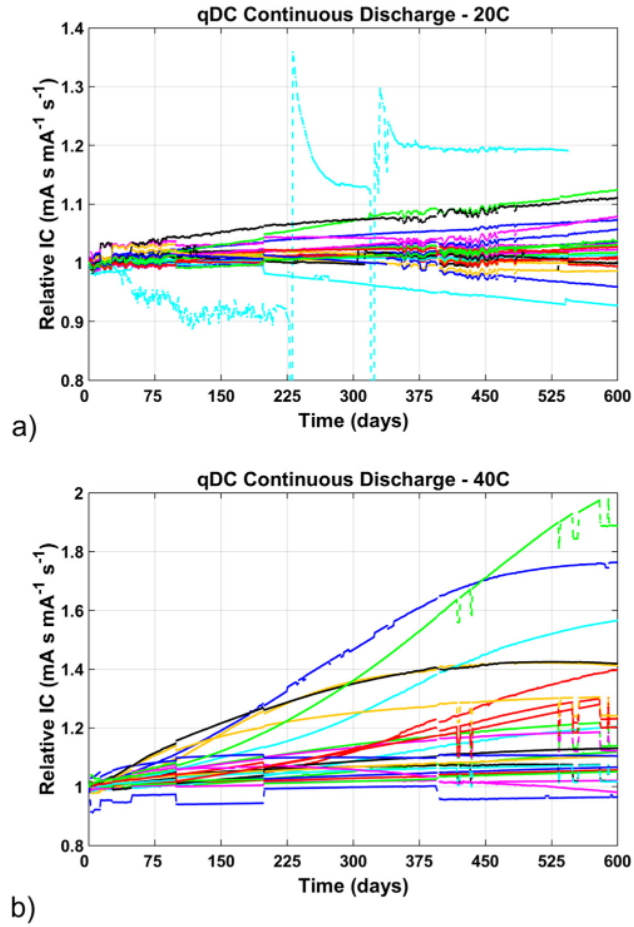

FIG. 11. Relative integrated current progression of the (a) qDC 20 °C UV LEDs after 600 days of continuous use and (b) qDC 40 °C UV LEDs after 600 days of continuous use.

promising metrics were the UV ratio, output power, ideality factor after turn-on, and 6V current. Few of the correlations of these metrics are strong, but of those considered, they are the best. One thing of note from the correlation table is that the pretest metrics have stronger correlations with the performance of the qDC LEDs than the pulsed LEDs. While this could be a byproduct of the way the groups were split up, this could also be explained by the fact that the qDC LEDs have consistently degraded more than the pulsed LEDs and that these pretest metrics have less influence on the early degradation of the devices and start to influence performance more as the LEDs lose more power.

TABLE III. Failure percentiles for the Monte Carlo lifetime simulation.

Failure percentile (%)	DC continuous failure time (days)	Pulsed continuous failure time (days)
5	527	3048
10	634	3249
25	891	3624
50	1461	4160

It is also worth mentioning that the correlation is only a measure of a linear dependence between two datasets. At a most basic level, the current-voltage and current-power relationships of these devices are nonlinear. Even worse, the quantities that were chosen to connect the initial presence of defects to optical power loss, such as the ideality factor or peak height ratio, are complex and have largely been uninvestigated to this point. Since the physics that governs the performance of these DUV LEDs is complex, it is reasonable that there are higher order relationships

between these pretest metrics and the long-term performance that are not obvious in the linear correlation. More complex analysis techniques may be needed in the future, but this linear analysis can still be a useful indication of long-term performance.

F. Partial least squares regression

Although the linear correlation showed no obvious trends between the pretest metrics and the change in IC after 600 days, developing a regression model is still a useful tool in predicting either the absolute power degradation of each device after a specific amount of time or, more importantly, looking at the projected performance of a device relative to the rest of the lot to pick devices that should have better long term performance. Since this lifetime test is driving the devices in a novel way compared to what is traditionally done in the literature, there is also no physics-based model from which to start. While it is clear that the relationships between the chosen performance metrics and the lifetimes of these devices is a complex one, it is simplest to start from a linear regression model and work to more complex models if needed.

A partial least squares regression model (PLSR),[59] was used to create two different models to predict the degradation of each device after 600 days of use. A quality indicators model was the first PLSR approach that was looked at. It used the prelifetime metrics presented in Table IV plus the temperature of the LED and a categorical variable that took a value of 0 for devices operated in the qDC operating mode and a value of 1 for LEDs operated in the pulsed mode. These last two environmental variables were included in the model so that a single model could be fit to all 96 devices. While future models could look at a more advanced method of accounting for the LED temperature and operating condition, simply adding these parameters onto the end of the predictor variables is a reasonable way to account for the device operating conditions. The response variable in this model was the relative integrated current after 600 days of operation.

This quality indicator PLSR model was trained on a randomly selected 50% of the data and the remaining 50% of the device metrics were used as a test set to evaluate the quality of the model. While this model generally predicted the performance of the bulk of the devices, it struggled to predict the performance of the outliers that are requiring more than a 20% increase in integrated current. Since there are so few outliers in the dataset after 600 days, it will be difficult for a single model to connect the behavior of the best and worst performing devices. The weights generated by the PLSR model for the first 5 of 14 components explained only 60% of the total variance seen in the response variable. These weights can be used to infer how different metrics are used by the model to influence the fitted response. The principle components of the PLSR model verify that a higher device temperature causes a higher relative integrated current, or more power loss, which is the expected behavior for these types of devices. The components also all show that LEDs operated in the pulsed mode (categorical value of 1) exhibit a reduced relative integrated current value compared

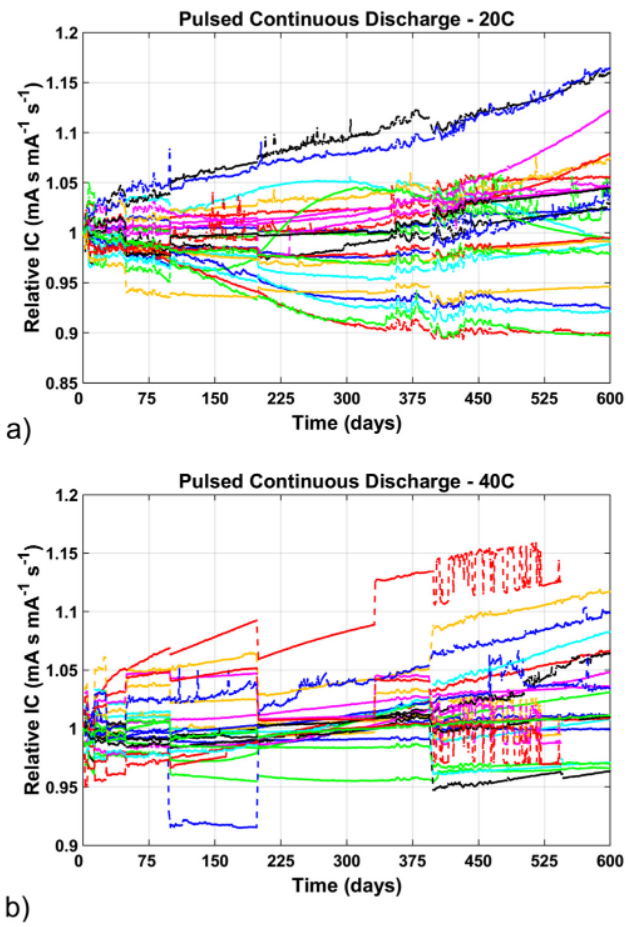

FIG. 12. Relative integrated current progression of the (a) pulsed 20 °C UV LEDs after 600 days of continuous use and (b) pulsed 40 °C UV LEDs after 600 days of continuous use.

TABLE IV. Correlation coefficients between each prelifetime metric and the relative increase in integrated current.

Metric	qDC, 20 °C	qDC, 40 °C	Pulsed, 20 °C	Pulsed, 40 °C
UV ratio	−0.536	−0.278	−0.153	−0.300
Low power	0.238	−0.396	0.293	−0.131
High power	0.176	−0.386	0.362	−0.220
Parasitic280	−0.182	0.512	0.161	0.121
Peak height ratio	0.050	0.081	0.003	0.116
IF_{off}	0.126	−0.186	−0.175	−0.429
IF_{on}	0.292	0.263	0.224	0.224
Leakage current	−0.384	0.171	0.015	−0.166
Pseudo-junction resistance	−0.039	−0.339	−0.093	0.060
4 V current	0.102	0.326	0.155	0.396
Turn-on current	0.159	0.083	0.085	0.386
6 V current	−0.286	0.278	−0.234	−0.047

to the qDC values (categorical value of 0), which makes sense since the qDC devices are generally degrading faster than the pulsed devices. The other information this model gives is that higher UV ratios (cleaner spectra) tend to lead to less degradation and the presence of a 280 nm parasitic peak increases the device degradation. The only other significant weights in the first 5 components are placed on the ideality factors before and after turn-on. Although the components seem to identify conflicting patterns in the ideality factor before turn on, the first principle component (most significant) indicates that higher ideality factors before turn on lead to reduced power loss while higher ideality factors after turn on lead to increased power loss. Both of these results are backed up by what is known in the device literature[27,60] in that degradation is caused by the same factors that lead to higher device turn-on currents (lower IF_{off}) and lower device efficiencies resulting from nonradiative recombination (higher IF_{on}). Even though the model does not perfectly predict the performance of these LEDs, the quality indicators PLSR model still generally reflects what is known about the physics of these devices, and this information can be used to roughly predict their long-term performance.

The other promising PLSR model that attempts to explain the long-term degradation of the continuous LEDs is different from the quality indicators model. It uses a single spectrum and I–V curve of a device to predict the performance. Even though the individual data points from a spectrum or I–V measurement of the device may be highly co-linear and contain more than 2000 measurements, the partial least squares algorithm is excellent at reducing the large number of predictor variables into a smaller number of uncorrelated components that can be used to predict the response variable. In this model, the matrix of predictor variables was a 96×2112 matrix where each row corresponds to a single sample, or LED, from the lifetime test, and each column corresponds to a measurement at a specific operating condition for all samples. A single row of the predictor matrix was comprised of the 2047 measurements of spectrum counts taken at 20 mA at uniformly spaced wavelengths between 185.8 and 757.7 nm, 63 measurements of the device current taken at uniformly spaced voltages between −6 and 6.4 V, and then the device operating temperature in °C. A Boolean, 0 or 1, corresponding to qDC or pulsed operation, was also used.

The resulting evaluation of the spectrum and I–V PLSR model can be seen in Fig. 13. This model predicts the relative IC after 600 days more precisely than the quality indicator model and is also able to predict the large degradation seen in the outliers more accurately than any other model. Several other PLSR models were looked at, including models that just used a spectrum measurement or just used an I–V curve of the LED, but using both the spectrum and I–V measurements of a single device gave the PLSR model much higher predictive power for the devices that had degraded more than average. The PLSR model was determined using only 15 principle components, which was enough to explain 98.9% of the variance in the response variable.

The first two components place a positive weight on the majority of the I–V curve after turn-on. The last five components place a negative weight on most or all of the I–V curve after turn-on, meaning a more efficient device should indicate higher long-term reliability. The last point about the spectra and IV PLSR model worth mentioning is that, as expected, the first component of the model places a positive weight on the operating temperature, indicating that hotter devices degrade faster. The most significant contributions also place a negative weight to the operating condition of the device, indicating devices run in the pulsed mode (categorical value of 1) typically degrade less than the qDC devices. Both of these checks indicate that the PLSR model can be backed by physics, and it is finding significance in the shapes of the pretest spectra and IV curves.

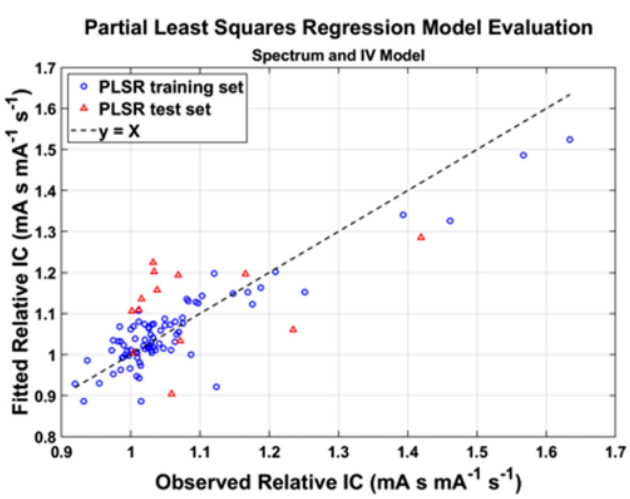

FIG. 13. Spectrum and IV PLSR model evaluation on the training and test datasets.

V. SUMMARY AND CONCLUSIONS

Testing of UV LEDs has been performed to characterize their performance over the entire expected operating range of the LISA charge management device. A pair of lifetime tests were performed to assess the reliability of the LEDs during both continuous and intermittent discharge modes. A first lifetime test observed the effects of a wide range of operating conditions on the degradation rates of four different lots of UV LEDs. After more than 180 days of testing, the parameter survey lifetime tests showed that UV LEDs would be able to perform intermittent discharge in both the continuous and pulsed operating modes with no concern of device failure. Even though the lifetime tests did not run long enough to see significant changes in the devices being operated at realistic spacecraft temperatures and driving conditions that simulated the continuous discharge modes, a Monte Carlo simulation was performed that provided confidence intervals for the expected lifetime of a UV LED being operated in either a DC or pulsed continuous discharge mode.

A second lifetime test is still evaluating the continuous discharge performance of another 96 LEDs, and the results thus far are showing that these UV LEDs, at realistic on-orbit temperatures, should be able to survive the 2 year target goal for the lifetime test,

meaning that with the redundancy of the LISA CMD, the UV LEDs should be able to perform continuous discharge for the nominal science mission duration with at least 2× redundancy. Pretest measurements of the physical characteristics of each of the LEDs were made and give insight into how the initial manufacturing quality of a device affects its long term performance. These pretest measurements were also used to create a partial least square regression model that can predict the long-term performance of the LEDs. Two different models were created, and both models show an agreement with the physics-based interpretations of the test results and validate that there is a relationship between the initial LED parameters and its long-term performance.

Our results show that state-of-the-art deep UV LED technology is ready to replace mercury-vapor lamps as the UV light source for contactless discharge in space. The long-term performance of UV LEDs can be reasonably predicted based on a few short tests run during initial device screening. More than 200 deep UV LEDs have been tested over a wide range of temperature and driving conditions to assess the instantaneous and long-term performance, and six UV LEDs have been tested in thermal vacuum inside a medium fidelity charge management device. After being tested over the full flight temperature envelope, the results show the LEDs meet all requirements of the CMD, while lifetime test results under both dc and pulsed conditions show they can fulfill the mission requirements.

ACKNOWLEDGMENTS

This work was supported by NASA Grant No. 80NSSC17K0277 and NASA Contract No. 80NSSC22K0288.

AUTHOR DECLARATIONS

Conflict of Interest

The authors have no conflicts to disclose.

Author Contributions

Benjamin C. Letson: Data curation (lead); Formal analysis (lead); Investigation (lead); Methodology (supporting); Software (lead); Supervision (lead); Validation (equal); Visualization (equal); Writing – original draft (lead). **Simon Barke:** Data curation (supporting); Formal analysis (supporting); Investigation (supporting); Software (supporting); Visualization (equal); Writing – review & editing (equal). **Peter Wass:** Conceptualization (lead); Formal analysis (supporting); Funding acquisition (supporting); Methodology (lead); Project administration (lead); Supervision (supporting); Validation (equal); Writing – review & editing (equal). **Guido Mueller:** Conceptualization (equal); Funding acquisition (supporting); Methodology (equal); Resources (equal); Supervision (equal); Writing – review & editing (equal). **Fan Ren:** Methodology (equal); Supervision (equal); Validation (equal); Writing – review & editing (equal). **Stephen J. Pearton:** Methodology (equal); Supervision (lead); Validation (lead); Writing – original draft (supporting); Writing – review & editing (lead). **John W. Conklin:** Funding acquisition (lead); Resources (lead); Supervision (equal); Validation (equal); Writing – review & editing (equal).

DATA AVAILABILITY

The data that support the findings of this study are available from the corresponding author upon reasonable request.

REFERENCES

[1]M. Armano *et al.* , Phys. Rev. Lett. **120**, 061101 (2018).
[2]R. A. Hulse and J. H. Taylor, Astrophys J. **195**, L51 (1975).
[3]B. P. Abbott *et al.*, Phys. Rev. Lett. **116**, 061102 (2016).
[4]G. M. Harry and LIGO Scientific Collaboration, Classical Quant. Grav. **27**, 084006 (2010).
[5]P. Amaro-Seoane *et al.* , "Laser interferometer space antenna," arXiv arXiv:1702.00786 (2017).
[6]R. Tso, D. Gerosa, and Y. Chen, Phys. Rev. D **99**, 124043 (2019).
[7]P. Wass and LISA Pathfinder Collaboration, "Free-fall performance for the LISA gravitational wave observatory: New results from LISA Pathfinder," in *APS April Meeting Abstracts*, APS Meeting Abstracts Vol. 2018 (April 14–17, 2018), p. C14.001; available at http://meetings.aps.org/link/BAPS.2018.APR.C14.1.
[8]D. Hollington, J. T. Baird, T. J. Sumner, and P. J. Wass, Classical Quant. Grav. **32**, 1 (2015).
[9]B. Christophe, D. Boulanger, B. Foulon, P. A. Huynh, V. Lebat, F. Liorzou, and E. Perrot, Acta Astronaut **117**, 1 (2015).
[10]T. Olatunde, "UV LED based charge control for the LISA gravitational reference sensor," Ph.D. thesis (University of Florida, 2018).
[11]C. W. F. Everitt *et al.* , Classical Quant. Grav. **32**, 224001 (2015).
[12]S. Buchman, W. Bencze, R. Brumley, B. Clarke, and G. M. Keiser, AIP Conf. Proc. **456**, 178 (1998).
[13]R. Dolesi *et al.* , Classical Quant. Grav. **20**, S99 (2003).
[14]M. Armano *et al.* , J. Phys. Conf. Ser. **610**, 012005 (2015).
[15]M. Armano *et al.* , Phys. Rev. Lett. **118**, 171101 (2017).
[16]G. P. Adams, G. K. Rochester, T. J. Summer, and O. R. Williams, J. Phys. E: Sci. Instrum. **20**, 1261 (1987).
[17]K.-X. Sun, B. Allard, S. Buchman, S. Williams, and R. Byer, Classical Quant. Grav. **23**, S141 (2006).
[18]S. Saraf *et al.* , Classical Quant. Grav. **33**, 245004 (2016).
[19]J. W. Conklin and The Gravity Probe B Collaboration, J. Phys. Conf. Ser. **140**, 012001 (2008).
[20]Y. Taniyasu, M. Kasu, and T. Makimoto, Nature **441**, 325 (2006).
[21]M. S. Shur and R. Gaska, IEEE T Electron. Dev. **57**, 12 (2010).
[22]J. Glaab *et al.* , J. Appl. Phys. **123**, 104502 (2018).
[23]Z. Bryan, I. Bryan, J. Xie, S. Mita, Z. Sitar, and R. Collazo, Appl. Phys. Lett. **106**, 142107 (2015).
[24]R. Gaska *et al.* , MRS Online **764**, C6.9 (2003).
[25]H. Amano *et al.* , J. Phys. D Appl. Phys. **53**, 503001 (2020).
[26]T.-C. Hsu *et al.* , Photonics **8**, 196 (2021).
[27]J. Glaab *et al.* , IEEE Photonic Technol. Lett. **31**, 529 (2019).
[28]D. Monti *et al.* , IEEE T Electron. Dev. **66**, 3387 (2019).
[29]N. Lobo-Ploch *et al.* , Appl Phys Lett **117**, 111102 (2020).
[30]N. Trivellin, D. Monti, C. De Santi, M. Buffolo, G. Meneghesso, E. Zanoni, and M. Meneghini, Microelectron. Reliab. **88–90**, 868 (2018), 29th European Symposium on Reliability of Electron Devices, Failure Physics and Analysis (ESREF 2018).
[31]N. Trivellin, D. Fiorimonte, F. Piva, M. Buffolo, C. De Santi, G. Meneghesso, E. Zanoni, and M. Meneghini, Electronics **11**, 728 (2022).
[32]J. Glaab *et al.* , J. Appl. Phys. **131**, 014501 (2022).
[33]N. Trivellin, M. Meneghini, M. Buffolo, G. Meneghesso, and E. Zanoni, IEEE T Device Mat Re **18**, 391 (2018).
[34]F. Piva *et al.* , Photonics Res. **8**, 1786 (2020).
[35]S. Sawyer, S. L. Rumyantsev, and M. S. Shur, Solid State Electron **52**, 968 (2008).
[36]C. G. Moe *et al.* , Appl. Phys. Lett. **96**, 213512 (2010).
[37]Y.-Z. Wang *et al.* , Appl. Phys. Lett. **116**, 203501 (2020).

[38]P. J. Wass, H. M. Araújo, D. N. A. Shaul, and T. J. Sumner, Classical Quant. Grav. **22**, S311 (2005).
[39]S. Saraf *et al.* , Classical Quant. Grav. **33**, 245004 (2016).
[40]V. Adivarahan, W. H. Sun, A. Chitnis, M. Shatalov, S. Wu, H. P. Maruska, and M. A. Khan, Appl. Phys. Lett. **85**, 2175 (2004).
[41]M. Meneghini, D. Barbisan, L. Rodighiero, G. Meneghesso, and E. Zanoni, Appl. Phys. Lett. **97**, 143506 (2010).
[42]M. Su, X. Zhu, Q. Guo, Z. Chen, S. Deng, Z. Chen, Y. Wang, J. Deng, and W. Sun, AIP Adv. **11**, 035315 (2021).
[43]Z. Ma, H. Cao, S. Lin, X. Li, and L. Zhao, Solid State Electron. **156**, 92 (2019).
[44]N. Trivellin, D. Monti, F. Piva, M. Buffolo, C. Santi, E. Zanoni, G. Meneghesso, and M. Meneghini, Jpn. J. Appl. Phys. **58**, SCCC19 (2019).
[45]A. Pinos, S. Marcinkevičius, J. Yang, R. Gaska, M. Shatalov, and M. S. Shur, J. Appl. Phys. **108**, 093113 (2010).
[46]H. Zhang *et al.* , IEEE Electr, Device L **42**, 978 (2021).
[47]C.-C. Lu, C.-P. Wang, C.-Y. Liu, and C.-P. Hsu, IEEE T Electron Dev. **63**, 3143 (2016).
[48]D. Monti *et al.* , IEEE T Electron. Dev. **66**(8), 1 (2019).
[49]C. Sah, R. N. Noyce, and W. Shockley, Proc. IRE **45**, 1228 (1957).
[50]H. Masui, Semicond Sci. Tech. **26**, 075011 (2011).
[51]J. M. Shah, Y.-L. Li, T. Gessmann, and E. F. Schubert, J. Appl. Phys. **94**, 2627 (2003).
[52]H. Masui, S. Nakamura, and S. P. DenBaars, Appl. Phys. Lett. **96**, 073509 (2010).
[53]D. Monti *et al.* , IEEE T Electron. Dev. **64**, 200 (2017).
[54]OptanLED: "TO-39 Ball Lens 250–280 nm UVC LED by Optan," https://www.optanled.com/products/optan-to-39-ball-lens (2020), Accessed: 2020-12-01.
[55]S. E. Technologies, "TO-Can 39 Series (TUDx9H1B)," http://www.s-et.com/upload2/TUD59H1B.PDF (2018), Accessed: 2020-12-01.
[56]B. C. Letson, "High volume UV LED performance testing," Submitted to Rev. Sci. Instrum. **93**, 114503 (2022).
[57]D. Hollington, J. T. Baird, T. J. Sumner, and P. J. Wass, Classical Quant. Grav. **34**, 205009 (2017).
[58]M. Shatalov, Z. Gong, M. Gaevski, S. Wu, W. Sun, V. Adivarahan, and M. A. Khan, "Reliability of AlGaN-based deep UV LEDs on sapphire," Proc. SPIE **6134**, 61340P (2006).
[59]MathWorks, see "Partial least squares regression and principal components regression," https://www.mathworks.com/help/stats/partial-least-squares-regression-and-principal.-components-regression.html (last accessed 3 March, 2022).
[60]G. Pedroza, L. Bechou, Y. Ousten, L. S. How, O. Gilard, J.-L. Goudard, and F. Laruelle, "Long term in-vacuum reliability testing of 980 nm laser diode pump modules for space applications" *2014 IEEE Aerospace Conference*, Yellowstone Conference Center, Big Sky, Montana, March 1–8, 2014 (IEEE, 2014), pp. 1–14.